Int. J. Heat Mass Transfer. Vol. 27, No. 9, pp. 1551–1557, 1984
Printed in Great Britain

0017-9310/84 $3.00 + 0.00

Film cooling effectiveness and turbulence distribution of discrete holes on a convex surface

SHAO-YEN KO, JING-ZHONG XU, YONG-QING YAO
Institute of Engineering Thermophysics, Chinese Academy of Sciences,
P.O. Box 2706, Beijing 100080, China

and

FU-KANG TSOU
Drexel University, Philadelphia, PA 19104, U.S.A.

(*Received* 14 *December* 1983)

Abstract—The flow fields near the exits of a row of film cooling holes on a convex surface have been measured extensively. The data measured include the velocity vector, wall static pressure distribution, turbulence profiles and film cooling effectiveness. Near the downstream edge of the hole, the recirculation zone induced by the mainstream around the jets was rather strong. Due to the curvature, the film jets had better attachment to the wall than to the flat plate for a blowing rate of $M < 1.0$. For $M > 1.0$, film jets 'separated' from the wall near the injection holes. A partially parabolic hypothesis has been used to predict the film-cooling flow field near the injection holes in a longitudinally curved channel.

1. INTRODUCTION

IN ORDER to better understand the film cooling effectiveness of discrete holes, it is necessary to make further studies of the flow field, heat and mass transfer, turbulence and pressure distributions near the exit region of film cooling holes. When the cooling jets are injected into the mainstream at a given angle (in the present case, the injection angle of the jet with the direction of mainstream is 30°), the jets and the mainstream interact with each other with recirculation and turbulence mixing in a complicated nature at the near hole region. Better film cooling effectiveness can be expected at a lower blowing rate, due to better and stable cooling film coverage at the near hole region. However, at a higher blowing rate, the cooling film flow momentum has a tendency to 'blow away' the cooling film from the wall. In order to design a better film cooled turbine blade for an advanced turbine, it is desirable to have a better understanding of the heat transfer characteristics of a row of film cooling holes along a curved surface for both the near-injection region and that further downstream. The downstream heat transfer nature is actually the extension and expansion of the near-injection region flow. Due to the 3-D nature of the computation at the near-injection region and the difficulties in measurements for such complicated flow, the published data are rather limited [1]. In the present paper, as shown in Fig. 1, experimental and numerical results are presented for film cooling at the exit region of discrete holes on a convex surface. The results include the distributions of the velocity vector, film cooling effectiveness, wall static pressure and turbulence distribution.

2. EXPERIMENTAL WORK

The experimental system is the same as described in ref. [2]. The test section of the heat transfer wind tunnel is 40 × 100 mm. The radius of curvature of the convex surface is $R = 130$ mm. The diameter, D, of film cooling holes is 10 mm and the angle of inclination is 30°. There are three holes in a line 20 mm apart. The maximum mainstream velocity was 47 m s^{-1}. The average turbulence level at the inlet of the test section was about 4%. Carbon dioxide was mixed with compressed air inside a premix tank before it was injected into the mainstream as the 'cooling' film. Carbon dioxide concentrations were measured with a conduction-type chromatograph with an accuracy of 0.2%.

The effectiveness for film cooling can be written as

$$\eta_T = (T_{aw} - T_\infty)/(T_2 - T_\infty) = f_T(Re, Pr, X) \quad (1)$$

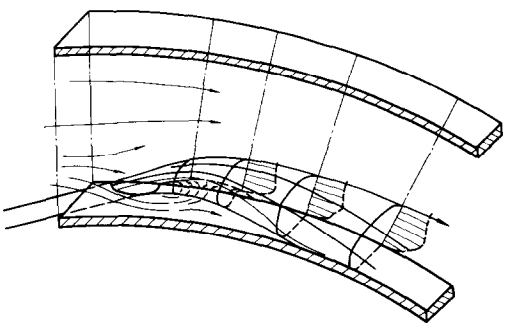

FIG. 1. Flow field at the exit region of discrete holes on a convex surface.

NOMENCLATURE

C_p	$2(P-P_{ref})/\rho_2 V_2 U_\infty$
D	diameter of the holes [mm]
K	turbulent kinetic energy, $1/2(u'^2+v'^2+w'^2)$ [$m^2 s^{-2}$]
M	blowing ratio, $\rho_2 U_2/\rho_\infty U_\infty$
P	static pressure [$N m^{-2}$]
P_{ref}	reference static pressure [$N m^{-2}$]
R	radius of wall curvature [mm]
Re_D	Reynolds number based on the diameter of the holes
Re_δ	Reynolds number based on the thickness of the upstream boundary layer
S_ϕ	source term of ϕ
U_∞	velocity of mainstream [$m s^{-1}$]
V_2	exit velocity of coolant [$m s^{-1}$]
x, ξ	streamwise distance from the upstream edge of the holes [m]
y, η	distance from the wall [m]
z, ζ	spanwise distance from the centreline [m].

Greek symbols

δ	thickness of boundary layer [m]
ε	turbulence dissipation function, $C_D K^{3/2}/L$ [$m^2 s^{-3}$]
η	film cooling effectiveness
$\nabla\xi, \nabla\eta, \nabla\zeta$	total length of the flow field in each direction [m]
ρ	density of coolant [$kg m^{-3}$]
ρ_∞	density of mainstream [$kg m^{-3}$]
ϕ	function.

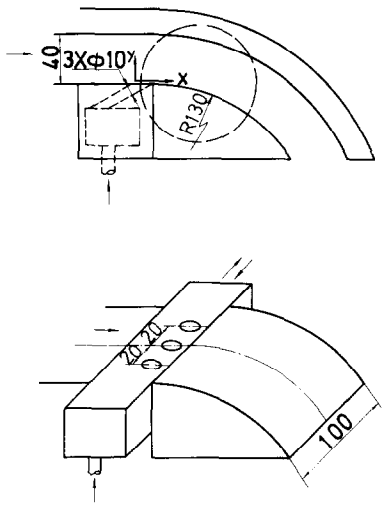

FIG. 2. Geometry of the test section.

where X is the injection hole geometry factor, including hole shape, dimension and injection angles.

If a foreign gas has been used for injection and the concentration distributions C_{wi} of foreign gas downstream of the injection hole on the wall of the testing convex surface have been measured, then the corresponding effectiveness should be in the form

$$\eta_m = (C_{wi}-C_\infty)/(C_2-C_\infty) = f_m(Re, Sc, X). \quad (2)$$

Thus when the Reynolds numbers are equal, the geometrical factor X the same, and $Sc = Pr$, then $f_T = f_m$. If the temperatures of the injection stream and the mainstream are the same, $T_\infty = T_2$, i.e. there is only mass transfer and no heat transfer occurs, then one gets

$$\eta_T = \eta_m = \eta. \quad (3)$$

In the present experimental investigation, $Sc = 0.94$, $Pr = 0.708$, $(T_\infty - T_2) < 0.3°C$, and these satisfy the similarity of heat and mass transfer. The density ratio of this experiment is limited $\rho_2/\rho_\infty = 1.075$–$1.277$.

Figure 2 shows the geometry of the test section.

The velocity and turbulence distributions were measured by a two-focus laser velocimeter. Magnitude and direction of the velocity and turbulence intensity in the x- and y-directions were obtained. The data at each measuring point were processed in the microcomputer using the statistical probability method. The accuracy of this system was within 1%. The wall static pressure was measured with a micro-pressure difference sensor.

Experiments were carried out for blowing ratios $M = 0.2, 0.35, 0.5, 0.75, 1.0$, and 1.5, respectively. The experimental range is summarized in Table 1.

3. EXPERIMENTAL RESULTS

3.1. *Static pressure*

Static pressure distributions along the convex surface downstream of the film cooling hole are shown in Fig. 3. The reference pressure, P_{ref}, is the static pressure at $x/D = 6$, where the pressure was quite stable along the x-direction. Immediately downstream of the

Table 1. Experimental range

	M					
	0.2	0.35	0.5	0.75	1.0	1.5
Re_D	1.71×10^4	2.24×10^4	2.25×10^4	1.90×10^4	1.75×10^4	1.13×10^4
Re_δ	5125	7840	9024	6066	5255	4513
ρ_2/ρ_∞	1.277	1.154	1.088	1.158	1.075	1.092

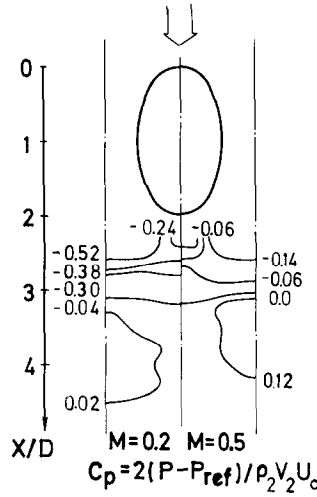

FIG. 3. Static pressure distributions along the convex surface.

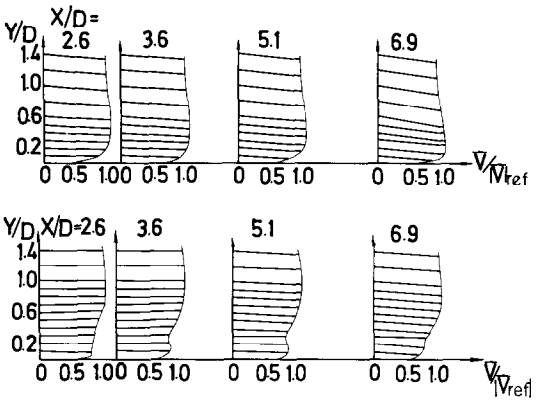

FIG. 5. Variation of velocity vectors at different x/D locations on the convex surface for $M = 0.5$.

injection hole, about $1.0D$ in length, there was a negative pressure region, which caused recirculation. Figure 4 shows the static pressure distributions along the centreline of the injection hole.

3.2. *Velocity distribution*

As shown in Fig. 1 the velocity distributions over the whole film cooling field near the injection holes up to $6.0D$ downstream were measured in detail with a laser velocimeter. Typical velocity vector variations at different x/D locations are given in Fig. 5 for $M = 0.5$. At $x/D = 3.6$ the film jet had the trend of departure from the wall in the $y/D = 0.2$ region. But further downstream, as $x/D = 6.9$ and $y/D = 0.2$, the film jet bent back to the convex wall until the jet reattached itself to the surface if the surface was long enough. The measurements of the velocity vectors showed the variation of the jet trajectory from 'separation' to reattachment.

3.3. *Profiles of turbulence distributions*

In Fig. 6, the profiles of $\sqrt{(\overline{u'^2})}/U_*$ and $\sqrt{(\overline{v'^2})}/U_*$ measured by a laser velocimeter are presented for $M = 0.5$, where U_* is the magnitude of the local velocity vector. The first observation is that the maximum of the turbulence intensities take place at the outside surface of the round jet, where the mixing between the jet and the mainstream is stronger. Within the extent of $y/D = 0.6$, the anisotropic features are apparent, but in the rest, the profiles appear to be isotropic. Maybe this observation proved that a simple isotropic turbulence model, such as the K–ε model, was not capable of handling the region very close to the exit of the jet.

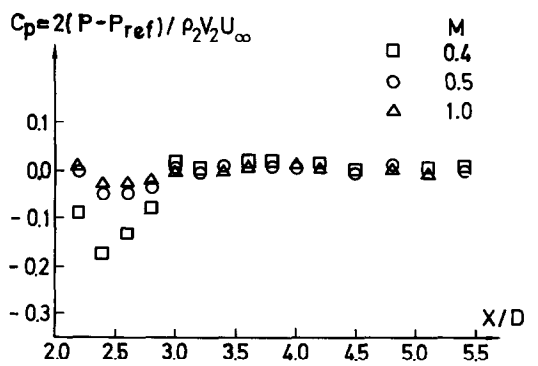

FIG. 4. Static pressure distributions along the centreline of the injection hole.

3.4. *Film cooling effectiveness*

Figure 7 shows the film cooling effectiveness at different x/D along the centreline of the film cooling hole. M-values varied from 0.5, 1.0, and 1.5. There are two regions which have different features. In the $x/D > 5$ region, the film cooling effectivenesses on the convex surface have a higher value than that on the flat plate for $M < 1.0$. However, for $M \geqslant 1.0$, the effectivenesses on the convex surface have a lower value than that on the flat plate. This conclusion coincides with that of Goldstein and Eckert [3]. While, in the region where $x/D \leqslant 5$, an opposite conclusion is obtained, that is, the effectivenesses have lower values on the convex surface for $M < 1.0$ but have higher values for $M \geqslant 1.0$. This may be because of the more intensive penetration in the vicinity of the downstream edge of the hole on the convex surface. However, when the blowing rate increases continuously, even though the penetration is more and more intensive, the effectiveness is still higher than that on the flat plate due to the increase of coolant mass flow rate. The location where η reaches a maximum value does not change when M varies from 0.5 to 1.5. But in the flat plate case [2], the maximum η point changes further downstream as M increases from $M = 0.5$ to 1.5 as indicated in the same figure.

Figure 8 shows the overall picture of the film cooling effectiveness distribution. In this figure, the $\eta = 0.20$ curves are plotted downstream of the injection hole at three different M-values. It can be seen clearly that near the hole injection region, a lower blowing rate, such as $M = 0.5$, gives a wider film cooling coverage and a

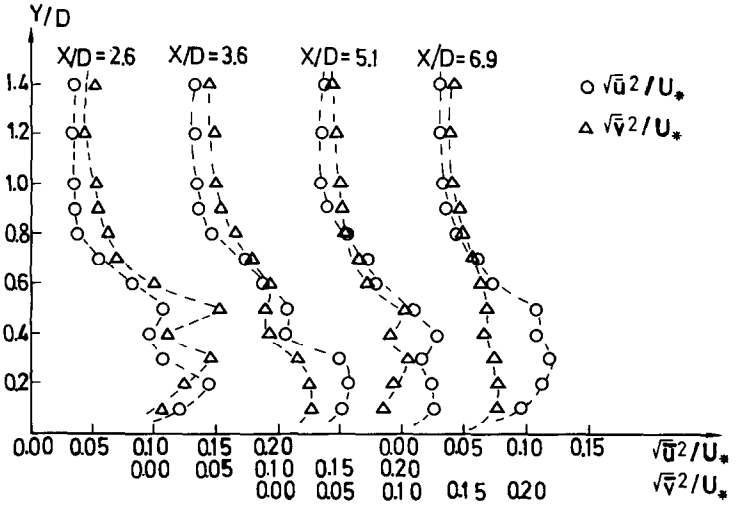

FIG. 6. Profiles of turbulence distributions for $M = 0.5$.

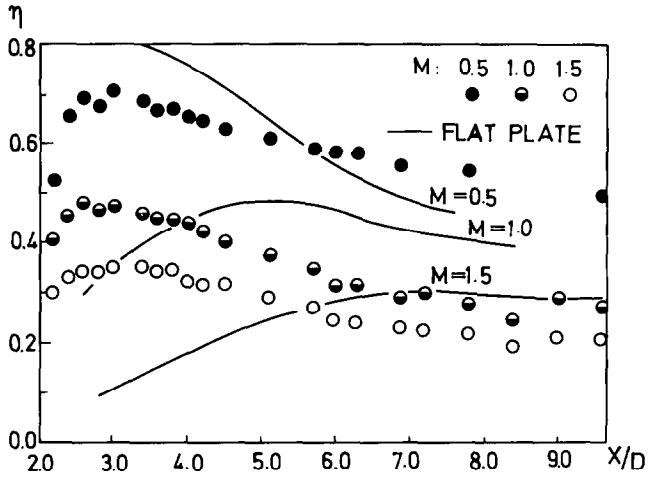

FIG. 7. η-values at different x/D, $M = 0.5$, 1.0, and 1.5.

higher film cooling effectiveness than a higher blowing rate. This conclusion indicates that for better film cooling over the convex surface of a turbine blade it would be better to use a lower blowing rate such as $M \leqslant 0.5$. At such a blowing rate, it will not only save cooling air considerably, but will also provide better film cooling protection.

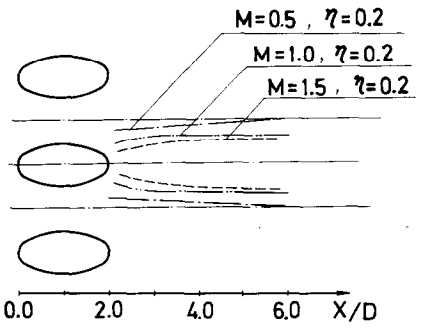

FIG. 8. Effect of M on surface contours of 20% effectiveness.

4. NUMERICAL ANALYSIS

As shown in Fig. 1, the region of numerical computation is defined in the longitudinally curved channel. The origin of the coordinate system is located two diameters upstream from the centre of the injection hole. The x-axis is chosen along the convex surface. The centreline of the injection hole lies in the x–y plane, and has an angle of 30° with the x-axis.

4.1. *Basic equations*

With the partially parabolic hypothesis, the conservation equation has the general form

$$\partial(\rho u\phi)/\partial x + \partial[(1+cy)(\rho v\phi - \Gamma_\phi \partial\phi/\partial y)]/\partial y + \partial[(1+cy)(\rho w\phi - \Gamma_\phi \partial\phi/\partial z)]/\partial z = S_\phi. \quad (4)$$

The continuity equation, three momentum equations, energy equation and two-equation type turbulent equations can be obtained by setting $\phi = 1, u, v, w, H, K$, and ε, respectively.

Table 2. Boundary conditions of different functions

	u	v	w	H	K	ε	p
Bottom surface	0	0	0	$\partial H/\partial x = 0$	0	0	—
Top surface	0	0	0	$\partial H/\partial y = 0$	0	0	—
Side plane	$\partial u/\partial z = 0$	$\partial v/\partial z = 0$	0	$\partial H/\partial z = 0$	$\partial K/\partial z = 0$	$\partial \varepsilon/\partial z = 0$	—
Exit of hole	u_2	v_2	w_2	H_2	K_2	ε_2	—

4.2. *Semi-orthogonal curvilinear coordinate system*

The Cartesian coordinate system x, y, z has been changed to the semi-orthogonal ξ, η, ζ curvilinear coordinate system by using the following relations

$$\xi = x \tag{5}$$

$$\eta = [(y-y_S)/(y_N-y_S)]^{1/2} \tag{6}$$

$$\zeta = (z-z_E)/(z_W-z_E) \tag{7}$$

where y_S is the coordinate of the bottom of the channel, y_N the coordinate of the top of the channel, z_E the symmetrical plane of the flow channel going through the centreline of the middle injection hole [4], and z_W the plane of symmetry between holes. Taking $y_S = 0$, $z_E = 0$, $y_N - y_S = \Delta\eta = f(x)$; $z_W - z_E = \Delta\zeta = \text{const.}$, the differential transformation relations are

$$\partial/\partial x = \partial/\partial\xi - (\eta/2\cdot\Delta\eta)(\mathrm{d}\Delta\eta/\mathrm{d}\xi)\,\partial/\partial\eta \tag{8}$$

$$\partial/\partial y = (1/2\eta\cdot\Delta\eta)(\partial/\partial\eta) \tag{9}$$

$$\partial/\partial z = (1/\Delta\zeta)(\partial/\partial\zeta). \tag{10}$$

The general partial differential equation in the coordinate system is

$$\begin{aligned}&(1/\Delta\eta\cdot\Delta\zeta)\cdot\partial(\Delta\eta\cdot\Delta\zeta\cdot\rho u\phi)/\partial\xi\\&+(1/2\eta\cdot\Delta\eta)\cdot\partial[(1+c\eta^2\cdot\Delta\eta)(\rho v\phi\\&-(\Gamma_\phi/2\eta\cdot\Delta\eta)\cdot\partial\phi/\partial\eta)\\&-\eta^2\rho u\phi\,\mathrm{d}(\Delta\eta)/\mathrm{d}\xi]/\partial\eta+(1/\Delta\zeta)\\&\cdot\partial[(1+c\eta^2\cdot\Delta\eta)(\rho w\phi-(\Gamma_\phi/\Delta\zeta)\\&\cdot\partial\phi/\partial\zeta)]/\partial\zeta = S_\phi.\end{aligned} \tag{11}$$

4.3. *Boundary conditions*

Typical 2-D turbulent flow profiles are assumed at the entrance of the curved channel [5]. At the exit section, all the variables computed in this program are parabolic in nature except the pressure, so that the downstream boundary conditions are not needed in the computations. The modified pressure equation is actually the Poisson equation with a simplified source term

$$\nabla^2 p' = S'_p. \tag{12}$$

The following integration must be satisfied

$$\int_\tau \nabla^2 p'\,\mathrm{d}\tau = \int_\tau S'_p\,\mathrm{d}\tau = \int_A \partial p'/\partial n\,\mathrm{d}A \tag{13}$$

where S'_p is the source term of mass addition at each grid point due to the unsatisfaction of conservation of mass.

The convergent results will be obtained when

$$S'_p \to 0. \tag{14}$$

From equation (13) one obtains

$$\partial p'/\partial n\,|_A = 0. \tag{15}$$

The boundary conditions of other functions are given in Table 2.

5. NUMERICAL RESULTS

The radius of curvature of the convex channel is $R = 200$ mm. The diameter of the injection hole is $D = 4$ mm, $R/D = 50$. The u-velocity distribution along the centreline of injection holes in the x–y plane is evaluated at $x/D = 2.2$, 3.0, 4.2, 5.0, and 5.8. The calculated results are given in Fig. 9. $U_\infty = 40$ m s^{-1} and the blowing rate $M = 0.2$. For the film cooling flow along a convex surface, the u-component which is very close to the surface decreases along the x-direction until $x/D \geqslant 4.2$. This trend indicates that the film cooling injection along the convex surface has a shorter adverse pressure region as compared to the flat plate calculation. Figure 10 is the comparison of the measured u-velocity profiles and the computed results with slightly different M-values. This figure shows the fair agreement between the present experimental and numerical results. In Fig. 11, Curve 'a' gives the numerical results of film cooling effectiveness η along the x/D direction at $M = 0.2$, $Re_D = 0.77 \times 10^4$, $\delta^*/D = 0.1$ and $R/D = 50$. Curve 'b' in Fig. 11 gives the numerical results of η–x/D for discrete hole film cooling along the flat plate in the similar film cooling range, the injection angle with the flat plate is 30°, $Re_D = 0.77 \times 10^4$, $\delta^*/D = 0.1$ and $M = 0.17$. The film cooling effectiveness along the convex surface is higher than that of the flat plate.

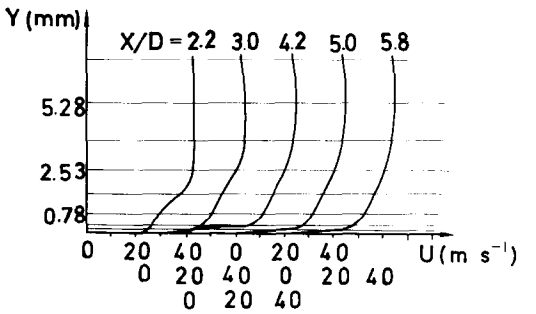

FIG. 9. u-Velocity distribution along the centreline of injection hole in the x–y plane.

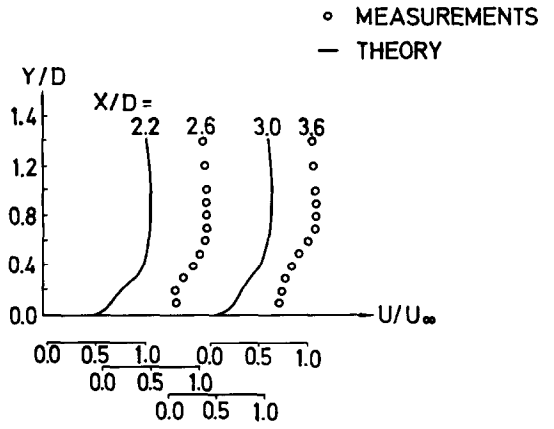

FIG. 10. Comparison of the measured u-velocity profiles with the computed results.

Curve 'c' is the experimental result given by Goldstein and Eckert [3] for $Re_D = 0.35 \times 10^3$, $R/D = 23$ and $M = 0.20$. As shown in Fig. 11 the cooling effectiveness η on the convex surface at the near injection hole is higher than that of the flat plate.

Figure 12 is the comparison of the present numerical and experimental results of effectiveness on the convex surface. It can be seen that the numerical results are reasonable as compared to that of experiments.

6. CONCLUSION

In the near injection hole region, for $x/D < 3$, or $1.0D$ downstream of the injection hole, the wall static pressure changed appreciably in both the streamwise and spanwise directions. This indicates the existence of

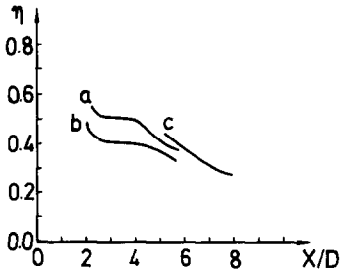

FIG. 11. Film cooling effectiveness in the x/D direction: (a) numerical results by the present authors on the convex surface; (b) numerical results by the present authors on the flate plate; (c) experimental results of Goldstein and Eckert [3].

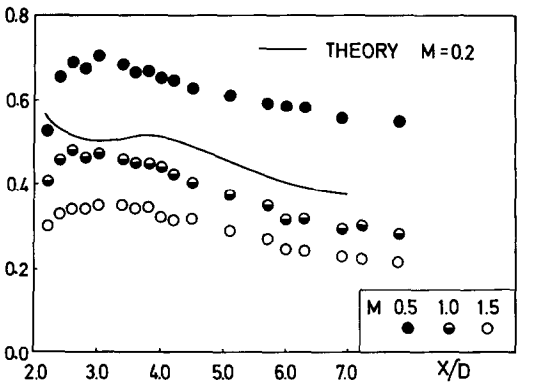

FIG. 12. Comparison of numerical and experimental results of effectiveness on a convex surface.

recirculation and film lifting effects. The conventional boundary-layer approach and 2-D calculations are not valid for this flow region. However, for the region further downstream, such as $x/D \geqslant 10$, the disturbances caused by the jets will decay, and the 3-D flow nature will be diminished gradually.

A coolant jet of lower blowing rate may give higher cooling effectiveness.

Film cooling of discrete holes over a convex surface may give better cooling effectiveness than a flat plate.

The measurements of the turbulence intensities indicate the existence of fairly large regions in which the turbulence field is anisotropic. This suggests that most of the commonly used isotropic turbulence model may not be capable of handling the flow in the region very close to the exit of the jet.

REFERENCES

1. G. Bergeles, A. D. Gosman and B. E. Launder, The turbulent jet in a cross stream at low injection rates: a 3-D numerical treatment, *Num. Heat Transfer* **1**, 217–241 (1978).
2. Shao-Yen Ko, Deng-Ying Liu, Yong-Qing Yao, Jin Li and F. K. Tsou, Film cooling effectiveness of discrete holes measured by mass transfer and laser interferometer, 7th Int. Heat Transfer Conf., Munchen, Federal Republic of Germany, Paper No. CP. 21, Vol. 6, September (1982).
3. R. J. Goldstein and E. R. G. Eckert, Film cooling of a gas turbine blade, *Trans. Am. Soc. Mech. Engrs*, Series A, *J. Engng Pwr* **100**, 476–481 (1978).
4. Jing-Zhong Xu and Shao-Yen Ko, Numerical computation for film cooling injection through discrete holes, *J. Engng Thermophys.* **4**, 67–73 (1983).
5. V. S. Pratap and D. B. Spalding, Numerical computation of flow in curved ducts, HTS/75/3, Imperial College, Mechanical Engineering Report, February (1975).

L'EFFICACITE DU REFROIDISSEMENT PAR FILM ET LA DISTRIBUTION DE LA TURBULENCE A TRAVERS UN TROU DISPERSIF A UNE SURFACE CONVEXE

Résumé—On a mesuré le champ de l'écoulement auprès d'une ligne de trous du refroidissement par film à la surface convexe. Les data mesurés incluent le vecteur de vitesse, la distribution de pression statique à la paroi, le profil de turbulence et l'éfficacité de refroidissement pat film. Au bord d'aval du trou, la zone de la recirculation introduite par le courant principal autour des jets est assez forte. A cause de la courbure, les jets de film attachés à la surface convexe sont meilleurs qu'à la surface plate, dans le taux de soufflage $M < 1.0$. Mais, pour $M \geqslant 1.0$, les jets de film se séparent de la paroi près des trous injecteurs. L'hypothès de la parabol partielle permet de prédire le champ de l'écoulement de refroidissement par film près des trous injecteurs au canal courbé.

UNTERSUCHUNGEN ÜBER FILMKÜHLUNG NEBEN DEM AUSTRITT DER DISKRETEN BOHRUNGEN AUF DER KONVEXEN WANDFLÄCHE

Zusammenfassung—Es wird das Strömungsfeld in der Nähe des Austritts einer Bohrungsreihe durch Filmkühlung auf der Konvexen Wandfläche ausführlich gemessen. Dadurch bekommende Daten enthalten Geschwindigkeitsvektor, statische Druckverteilung auf der Wand und Filmkühlungs wirksamkeit. In der Nähe Stromsunterlaufes der Höhle ist die Umströmungszone, die von Hauptströmung um Strahl veranlässt, immer noch recht stark. Infolge der Wallskrümmung Knüpft die Filmstrahl für $M < 1.0$ mit der Wand besser als mit Flachplatte an. Für $M \geqslant 1.0$ trennt Filmstrahl neben der Bohrung von der Wand. Partielle parabolische Hypothese wird zum Vorhersagen des Filmkühlströmungsfeldes bei den Einspritzbohrungen in einen longitudinalen krummen Kanal benutzt.

ЭФФЕКТИВНОСТЬ ПЛЕНОЧНОГО ОХЛАЖДЕНИЯ И РАСПРЕДЕЛЕНИЕ ТУРБУЛЕНТНОСТИ НА ДИСКРЕТНЫХ ОТВЕРСТИЯХ НА ВЫПУКЛОЙ ПОВЕРХНОСТИ

Аннотация—Проведено детальное исследование полей течения у выходных сечений ряда отверстий для пленочного охлаждения на выпуклой поверхности. Измерялись вектор скорости, распределение статического давления на стенке, профили турбулентности и эффективность пленочного охлаждения. У края отверстия вниз по потоку наблюдалась довольно интенсивная зона рециркуляции вокруг струй, вызванная основным потоком. При интенсивности вдува $M < 1,0$ пленочные струи лучше прилипали к выпуклой стенке, чем к плоской пластине. При $M > 1,0$ струи «отрывались» от стенок вблизи отверстий. Для расчета полей течения у отверстий для пленочного охлаждения в канале, изогнутом в продольном направлении, использовалась частично параболическая гипотеза.